Optical and magneto-optical properties of Co/Pt multilayers

S. Uba, L. Uba, A. N. Yaresko,* and A. Ya. Perlov*
Institute of Physics, Warsaw University Branch in Bialystok, Lipowa 41, PL-15-424 Bialystok, Poland

V. N. Antonov
Institute of Metal Physics, 36 Vernadskii strasse, 252142 Kiev, Ukraine

R. Gontarz
Institute of Molecular Physics, Polish Academy of Sciences, Smoluchowskiego 17, PL-60-179 Poznan, Poland
(Received 31 July 1995; revised manuscript received 20 October 1995)

Optical and magneto-optical spectral properties have been studied both experimentally and theoretically for a series of Co/Pt multilayers. Diagonal and off-diagonal components of the optical conductivity tensor have been determined in the photon energy range 0.8–5.5 eV from the polar Kerr rotation and ellipticity and the ellipsometry measurements. On the basis of self-consistent spin-polarized relativistic linear muffin-tin orbital band-structure calculations within the local spin-density approximation the conductivity tensor has been evaluated and the role of the spin-orbit interaction and the induced polarization effect at the multilayer interface in the formation of the magneto-optical activity has been studied for various model Co-Pt multilayers and alloys. The relevance of the interface alloying effect for the explanation of the experimental results has been examined and discussed.

I. INTRODUCTION

In the past several years, artificial layer structures composed of transition magnetic metals separated by nonmagnetic metals have intensively been studied due to the fundamental research interest in these systems and also because of their potential for applications. Oscillatory interlayer exchange coupling,[1] giant magnetoresistance,[2] and induced magnetic polarization effect in nonmagnetic layers (see, e.g., Ref. 3 and references therein) have become the most discussed phenomena in layered magnetic structures. In particular, Co/Pt multilayered structures (MLS) have attracted a lot of attention because these systems exhibit simultaneously a large magneto-optical (MO) Kerr rotation[4,5] and perpendicular anisotropy[6] which makes these materials applicable for a new generation of storage devices.[7]

A number of experimental investigations of the MO properties of Co/Pt MLS[4,5,7–10] prepared by different techniques show that the MO polar Kerr rotation spectra of Co/Pt MLS display a two-peak structure as an overall feature. The amplitude of the peak located at 1.5 eV is sensitive to the Co sublayer thickness, whereas the maximum observed at around 4 eV depends relatively weakly on both Co and Pt thicknesses and its amplitude overcomes the corresponding pure Co one, being slightly shifted to a higher energy.

One possible way to interpret the MO spectra is to use a macroscopic approach (see, e.g., Refs. 11 and 12). This approach is based on solving the equations of electromagnetic wave theory in the four component periodic medium Pt-interface-Co-interface. The unknown width and dielectric tensor of the interface is determined by the best fit to the experimental data.[5,9,12,13] Despite the obvious successes of such an approach the nature of the interface layers remains undefined and may be attributed to either ''magnetic Pt'' layer or some ''interface alloy'' layer.[8–10] Besides, this approach cannot elucidate the origin of the Kerr effect which is due to the interplay of magnetization and spin-orbit coupling (see, e.g., Ref. 14). Such an explanation arises only from the microscopic theory of MO properties. Recently developed techniques of *ab initio* calculations give good results for a wide class of transition metals compounds (see, e.g., Refs. 15–19).

The aim of this paper is a detailed investigation of the electronic structure of Co/Pt MLS via both experimental and theoretical studies of their optical and MO spectra. Some preliminary results on this subject have been published in our previous paper.[17]

To associate the electronic structure with MO properties it is inconvenient to consider the MO Kerr effect (MOKE) spectra. The complex Kerr rotation angle is composed of both diagonal and off-diagonal optical conductivity tensor (σ) components in a rather complicated way. On the other hand, it is well known that the absorptive part of the tensor only, but not the Kerr rotation itself, is directly connected with the optical transitions between electronic states, their strengths, and energy positions. Therefore, together with MOKE measurements we realized ellipsometric measurements of the diagonal part of the dielectric tensor and recalculated σ_{xx} and σ_{xy} components of the optical conductivity tensor.

It is presently impossible to carry out *ab initio* calculations of the optical and MO properties of realistic MLS because these are not monocrystalline materials with a well-defined structure. Therefore, in the theoretical part of the paper we investigate some idealized model structures representing the actual Co/Pt MLS. This simplification allows us nevertheless to clarify the main features in the formation of MO spectra of the MLS under consideration.

The paper is organized as follows. In Sec. II A experimental details are described: the sample preparation and charac-

TABLE I. The parameters of the Co/Pt MLS studied. No. is the sample number, N_{layers} is the number of bilayers, t_{Co} (t_{Pt}) are measured thicknesses of Co (Pt) sublayer.

No.	N_{layers}	t_{Co} (Å)	t_{Pt} (Å)
1	50	4.6	13.6
2	47	5.8	15.2
3	43	6.9	12.5
4	40	9.0	14.4
5	33	18.9	14.3

terization and the experimental setup for the sample properties measurements by spectroscopic ellipsometry and MO Kerr spectroscopy. The theoretical background of the *ab initio* calculations of the band structure and the optical conductivity tensor are reviewed in Sec. II B. In Sec. III experimental results for polar Kerr rotation and ellipticity spectra are presented, and also the spectra of the conductivity tensor components are determined and discussed. In Sec. IV A the results on the band-structure calculations for chosen model multilayers and alloys are presented, and the effects of hybridization, spin-orbit coupling, and effective magnetic field on the density of states projected on different sites inside and at the interface of constituent sublayers are discussed. The optical and MO properties calculated for pure Co and for the idealized Co/Pt MLS studied are described, compared with the measured ones, and discussed in Sec. IV B.

II. EXPERIMENTAL AND COMPUTATIONAL DETAILS

A. Experimental procedure

The Co/Pt MLS were deposited by face-to-face dc sputtering on water-cooled glass substrates in an automated and computer-controlled deposition system. Typical sputtering conditions and other technical details can be found in Ref. 20. The films' structure was determined by standard Θ-2Θ x-ray diffraction with Co-K(α) radiation. The layered structure was confirmed by low-angle x-ray diffraction (XRD). The modulation period was deduced from the position of the Bragg peaks. From the high-angle XRD a pronounced (111) texture was inferred. The sublayer thicknesses were determined by x-ray fluorescence analysis with energy dispersive x-ray (EDX) system. The total thicknesses of the Co and Pt layers were determined from the peak intensities of the characteristic fluorescence of Co-K(α) and Pt-K(α) radiation. The parameters of the samples studied are given in Table I.

The polar Kerr rotation (θ_K) and ellipticity (η_K) spectra were measured with a MO spectrometer based on the polarization modulation technique[21] in the photon energy range 0.8–5.5 eV. Light from a super quiet Xe arc lamp or D_2 lamp used in the uv region is focused via a condenser on the entrance slit of the monochromator (SPEX 500M) equipped with self-interchangeable gratings for the measurements of different parts of the spectrum. The outcoming light beam is filtered by an appropriate filter to attenuate higher orders from the monochromator. After passing through the polarizer and photoelastic modulator (Hinds PEM-90 CaF_2) the light beam is focused by a quartz lens on the sample surface mounted on the sample holder with temperature stabilized in the range 290–800 K inside of the 1.8 T water-cooled electromagnet. The amplitude of the retardation of the light is periodically modulated at the frequency of 57 kHz by the modulator oriented with its strain axis at 45° with respect to the polarizer axis. The angle of incidence of the light on the sample surface is 3°. After reflection the light beam passes through the analyzer oriented parallel to the modulator strain axis and is detected by a low-noise photomultiplier in the energy range $1.4 < h\nu < 5.5$ eV and by a liquid-nitrogen-cooled Ge diode for $0.8 < h\nu < 1.4$ eV. The detector output signal from the current preamplifier is measured by lock-in amplifiers. The polar Kerr rotation and ellipticity, after appropriate calibration with the use of a driven Babinet-Soleil compensator, are derived from the ratio of total light intensity, corrected for zero offset with the use of a controlled light beam shutter, and the intensity of the first and second harmonics. The same setup is used to measure θ_K and η_K hysteresis loops at fixed light wavelength. The setup is fully automated and computer controlled via an acquisition data system (Keithley 500A). The sensitivity of the Kerr spectrometer is of the order of 10^{-4} deg.

The optical properties—refractive index n and extinction coefficient k—have been measured by spectroscopic ellipsometry using the rotating analyzer method[22] in the spectral range 0.8–5.5 eV. The sample is mounted on a five-axis precision goniometer in the subset of the above-described MO system. The ellipsometric angles Ψ and Δ have been derived from the on-line digital harmonic analysis of the detected signal modulated by a rotating analyzer. The MgF_2 Rochon analyzer rotates with an angular frequency of 12 s^{-1} inside a rotary encoder with 4096 lines per revolution. The signal from the detectors is synchronously digitized at 20 μs intervals by the Keithley 500A system and on-line evaluated using the Hadamard transform. The angle of incidence has been set at 67°, optimized as averaged principal angle of incidence for the measured samples and the spectral range used. The accuracy of the angle of incidence setting is 0.005° and the average error in the determination of n and k values is of the order of 0.003.

B. Theory and computational details

Self-consistent band-structure calculations were carried out using the spin-polarized relativistic (SPR) linear muffin-tin orbital (LMTO) method.[23] A detailed description of the relativistic extension of the LMTO method was given elsewhere.[24] The four-component basis functions were constructed starting from the solution of the single-site Dirac equation for the spin-independent part of the effective one-electron potential. The matrix elements of the effective magnetic field were incorporated into a Hamiltonian at the variational step as proposed in Ref. 25. The choice of the basis functions makes it straightforward to construct the (third-order) LMTO Hamiltonian and to include the combined corrections to the atomic sphere approximation (ASA),[23] which are necessary to calculate accurately the conductivity tensor in a wide energy interval.[15,26] It has been shown[25,18] that in the ASA the perturbative approach is practically as accurate as the SPR LMTO method based on the proper solution of the single-site Dirac equation for a spin-dependent potential.

MO properties, in particular the MOKE, depend on both diagonal and off-diagonal components of the conductivity

tensor $\sigma_{\alpha\beta}(\omega)$. For the polar geometry and a solid with at least threefold rotational symmetry, the complex MO Kerr angle $\phi_K=\theta_K+i\eta_K$ is given by[27,28]

$$\phi_K=\frac{-\varepsilon_{xy}}{(\varepsilon_{xx}-1)\sqrt{\varepsilon_{xx}}}=\frac{-\sigma_{xy}}{\sigma_{xx}\sqrt{1+i(4\pi/\omega)\sigma_{xx}}}, \tag{1}$$

where $\varepsilon_{\alpha\beta}=\delta_{\alpha\beta}+i(4\pi/\omega)\sigma_{\alpha\beta}$ is the dielectric constant tensor.

Using the random-phase approximation, and neglecting the local-field effects the interband contribution to the absorptive part of the macroscopic conductivity tensor can be related to microscopic optical transitions by[29,30]

$$\sigma^{(1)}_{\alpha\alpha}(\omega)=\frac{\pi}{\hbar\omega}\sum_{\mathbf{k}}\sum_{ln} j^{\alpha}_{ln\mathbf{k}}j^{\alpha}_{nl\mathbf{k}}\delta(\omega_{nl}-\omega), \tag{2}$$

$$\sigma^{(2)}_{\alpha\beta}(\omega)=\frac{\pi}{\hbar\omega}\sum_{\mathbf{k}}\sum_{ln} \mathrm{Im}(j^{\alpha}_{ln\mathbf{k}}j^{\beta}_{nl\mathbf{k}})\delta(\omega_{nl}-\omega), \tag{3}$$

where $\sigma^{(1)}_{\alpha\beta}$ ($\sigma^{(2)}_{\alpha\beta}$) denotes the real (imaginary) part of $\sigma_{\alpha\beta}$, $j^{\alpha}_{ln\mathbf{k}}$ is the projection of the current density matrix element vector along the direction α of the electric field, and $\hbar\omega_{nl}=E_n(\mathbf{k})-E_l(\mathbf{k})$ is the energy difference between the unoccupied band n and the occupied band l. With $\psi_{n\mathbf{k}}(\mathbf{r})$ being the four-component Bloch wave function, the current density vector $\mathbf{j}_{ln\mathbf{k}}$ is defined by:

$$\mathbf{j}_{ln\mathbf{k}}=\int \psi^{\dagger}_{n\mathbf{k}}(\mathbf{r})(ec\boldsymbol{\alpha})\psi_{l\mathbf{k}}(\mathbf{r})d\mathbf{r}, \tag{4}$$

where c is the velocity of light and $\boldsymbol{\alpha}$ is the standard Dirac matrix. A detailed description of the formalism of evaluation (4) with the relativistic LMTO eigenfunctions and including the combined correction terms was given elsewhere.[26] Neglecting the integral over the interstitial region when evaluating expression (4) results in quite erroneous $\omega\sigma^{(2)}_{xy}$ spectra.[15,18,26] The main cause of the errors is the discontinuity of the LMTO ASA wave functions at the sphere boundary.[31,18] To avoid these errors, the authors of Ref. 18 have proposed to use an alternative form of the current density matrix elements. In our opinion, however, it is more rigorous to calculate (4) using continuous wave functions obtained from calculations with the combined corrections taken into account. Besides, the inclusion of the combined corrections in the LMTO Hamiltonian and overlap matrices results in more accurate band energies.

Once the $\mathbf{j}_{ln\mathbf{k}}$ is computed, expressions (2) and (3) are evaluated by the standard tetrahedron method.[32] The dispersive part of the conductivity tensor is then obtained via the Kramers-Kronig transformation. The lifetime effects are simulated by broadening the calculated spectra with a Lorentzian of width δ, with δ being interpreted as an inverse relaxation time. Finally, we take into account the intraband contribution to the diagonal part of the conductivity tensor which is given by the phenomenological Drude term

$$\sigma_{\mathrm{intra}}=\frac{1}{4\pi}\frac{i\omega_p^2}{\omega+i\gamma}, \tag{5}$$

with γ being a phenomenological intraband inverse relaxation time, and ω_p^2 being the squared plasma frequency. In all the calculations we used the same values $\gamma=0.05$ eV and $\delta=0.3$ eV for intra- and interband inverse relaxation time, respectively. The small intraband contribution[33] to the off-diagonal conductivity was neglected in the present calculations.

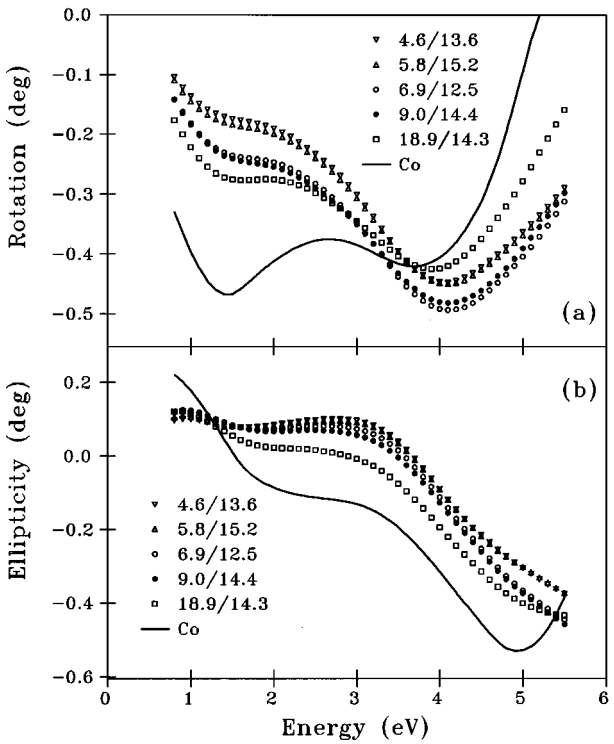

FIG. 1. Experimental polar Kerr rotation (a) and ellipticity (b) spectra of Co/Pt MLS and fcc Co film. Sublayer thicknesses marked in the pattern are given as t_{Co}(Å)/t_{Pt}(Å).

III. EXPERIMENTAL RESULTS

In order to discuss the origin of the MOKE in Pt-based multilayers in detail, we have measured optical and MO spectra for a wide range of photon energies for the series of MLS with sample parameters listed in Table I. As the MOKE is affected by both diagonal and off-diagonal components of the conductivity tensor, the appropriate discussion of electronic transitions underlying MO effects requires the analysis of the spectral dependencies of the tensor. From the measured complex polar Kerr angle and ellipsometric data we obtained the tensor components according to (1).

The measured polar Kerr rotation and ellipticity spectra of the Co/Pt MLS studied are shown in Fig. 1. All samples measured possess well-defined MOKE hysteresis curves with saturation characteristics and all θ_K and η_K spectra were measured under saturation conditions. The Kerr rotation spectra display two well-known features. There is a prominent broad negative peak in the uv region and a smaller one in the ir part. The ir peak, centered at 1.5 eV is most prominent for a pure Co thick film[34] and for MLS its amplitude continuously diminishes with decreasing MLS Co sublayer thickness. The uv peak slightly varies in energy position from 4.1 to 3.9 eV with increasing Co sublayer thickness. The uv peak amplitude overcomes that of pure Co film cen-

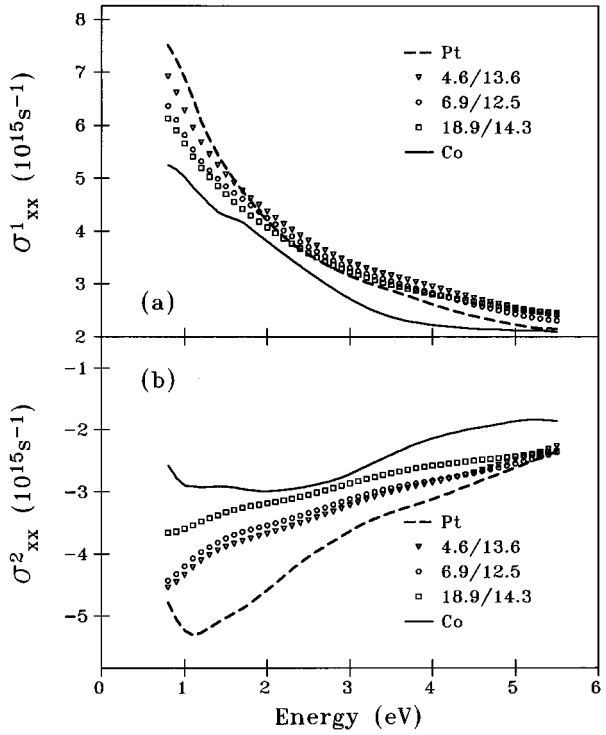

FIG. 2. The absorptive (a) and dispersive (b) parts of the diagonal components of the conductivity tensor for Co/Pt MLS and Co and Pt films, determined from the ellipsometric measurements.

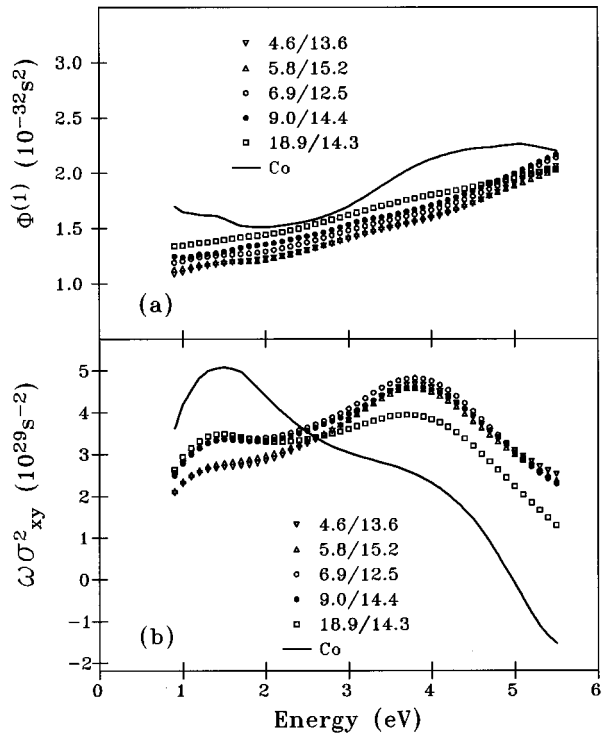

FIG. 3. The contribution to the Kerr rotation spectra from the diagonal part of the conductivity tensor (see text) (a), and (b) the absorptive part of the off-diagonal component $\omega\sigma_{xy}^{(2)}$, determined from the ellipsometric and the complex polar Kerr angle measurements for Co/Pt MLS and Co film.

tered at 3.7 eV and its amplitude relatively weakly depends on the composition of the MLS studied.

The characteristic feature in the Kerr ellipticity spectra is the shift of the zero crossing from 1.5 eV in pure Co film to 3.7 eV in MLS with decreasing Co sublayer thickness and the formation of a positive peak around 3 eV. The prominent minimum of the Kerr ellipticity centered at 4.9 eV observed in Co film presumably shifts its position to the photon energy region $\hbar\omega > 5.5$ eV, inaccessible in the present experiment.

The optical properties of the MLS, in the form of spectral dependencies of the diagonal component of the effective optical conductivity tensor σ_{xx}, are shown for the real $\sigma_{xx}^{(1)}$ and imaginary part $\sigma_{xx}^{(2)}$ in Fig. 2(a) and Fig. 2(b), respectively. For clarity, in the picture the spectra of only three samples are shown and the other MLS spectra are located in between them. As it is seen from the results, generally there are little differences in the absorptive part of the optical conductivity $\sigma_{xx}^{(1)}$ for all MLS studied. The magnitudes of the spectra are roughly scaled with the thickness of Co sublayers. The corresponding spectra of thick Co and Pt films prepared by the same technique are shown for comparison. It can be observed that the $\sigma_{xx}^{(1)}(\omega)$ curves for the MLS are not located between the Co and Pt one in the energy range 2–5.5 eV. Several reasons can be considered for this difference. A common problem in metal optics is a great sensitivity of the optical constants on the state of the sample surface.[35] Another cause can be the fact that the optical properties of thick metal films are slightly different from the ones for MLS constituent sublayers.[36] In other words, for individual layer thicknesses of a few atomic monolayers the effective dielectric constants of the medium differ from the dielectric constants of bulk or thick film material. Besides, the response of an ultrathin medium to an electromagnetic wave is substantially influenced by the electronic interaction with adjacent layers. The spectra of the dispersive part of the optical conductivity tensor $\sigma_{xx}^{(2)}$ are also weakly dependent on the MLS composition and are located nearly in between the spectra for thick Co and Pt films.

To separate the contribution to the MOKE coming from the diagonal and off-diagonal conductivity tensor components the function $\Phi = 4\pi[(\varepsilon_{xx}-1)\sqrt{\varepsilon_{xx}}\omega^2]^{-1}$ has been evaluated from the optical measurements. The real part of the function $\Phi^{(1)}$ is shown in Fig. 3(a). It has been found that for the compounds under consideration, the product of $\Phi^{(1)}$ and $\omega\sigma_{xy}^{(2)}$ gives a main contribution ($>80\%$) into the polar Kerr rotation spectra. It should be noted that this function is nearly flat over the investigated spectral region for all MLS studied and weakly dependent on their composition. On the contrary, the shape and the amplitude of the $\Phi^{(1)}$ spectrum change significantly in the case of Co film. As a consequence, the absorptive part of the off-diagonal component of the conductivity tensor, $\omega\sigma_{xy}^{(2)}$, presented in Fig. 3(b) for the MLS studied is in the overall form unexpectedly similar to the polar Kerr rotation, whereas for the case of pure Co the shape of the polar Kerr rotation and $\omega\sigma_{xy}^{(2)}$ differ significantly. Inspection of these curves shows that the presence of Pt leads to the strong enhancement of the $\omega\sigma_{xy}^{(2)}$ in the uv range. The enhancement of the polar Kerr rotation measured is much smaller due to the corresponding increase of the diagonal part of σ [see Fig. 3(a)].

Thus, it can be concluded that the peak observed in the ir part of the Co/Pt MLS polar Kerr rotation spectra can be related mainly to the MO activity of Co. On the contrary, the peak observed in the uv region is for pure Co connected rather with the peculiarities in the diagonal part of the conductivity tensor, while for Co/Pt multilayers it is governed by the off-diagonal component of σ and originate from Co-Pt interaction at the MLS interface. The multilayer MOKE spectra measured are qualitatively similar to the spectra which have been published for Co/Pt MLS prepared by different techniques and for random fcc Co-Pt alloys[4,5,7–10] and all exhibit similar MOKE enhancement in the uv region.

IV. THEORETICAL RESULTS AND DISCUSSIONS

A. Electronic structure

In order to reproduce the electronic structure of the interlayer interface we have performed the band-structure calculations of some model ordered Co-Pt alloys and nCo/mPt MLS, where $n(m)$ are the numbers of atomic planes. We assumed an $abcabc$ stacking sequence of closely packed planes corresponding to the fcc-(111)-texture for all the MLS structures except for 1Co/1Pt for which the $ababab$ stacking has also been studied. No attempt has been made to optimize the interlayer spacing, which was taken to be corresponding to ideal c/a ratio. Ordered $CoPt_3$ and Co_3Pt alloys were calculated in Cu_3Au crystal structure, while for CoPt alloy AuCu structure was used. For all the compounds the mean volume per atom was chosen to be equal to the average of atomic volumes of pure fcc Pt and hcp Co with the experimental lattice constants. The radii of Co and Pt atomic spheres were chosen to be equal to 1.46 Å. The LMTO basis functions with angular momentum up to $l=3$ for both cobalt and platinum spheres were retained in the decomposition of the Bloch wave function.

The ''frozen-core'' approximation was adopted. Exchange and correlation contributions to both atomic and crystalline potential were included through the density-functional description in the local spin-density approximation (LSDA) of von Barth–Hedin.[37] Brillouin zone (BZ) integrations were performed using the improved tetrahedron method.[38]

The characteristic feature of the electronic structure of Co/Pt multilayers and alloys is the strong hybridization of Co $3d$ and Pt $5d$ states, the latter being much more delocalized. Figure 4 shows the spin- and site-projected densities of the electronic states (DOS) for Co and Pt site in 2Co/1Pt, 1Co/1Pt, and 1Co/2Pt multilayers. The valence band width in the MLS is mainly governed by Pt d-d hybridization in the close-packed planes consisting of Pt atoms and varies moderately with an increase of the Pt sublayer thickness. Strong spin-orbit interaction in the Pt atomic sphere results in splitting of $d_{3/2}$ and $d_{5/2}$ states with the energy difference between their centers being ~ 1.5 eV. Inside the Co atomic sphere the effect of the spin-orbit coupling is much weaker than the effect of the effective magnetic field. The centers of both Pt $d_{3/2}$ and $d_{5/2}$ states lie at lower energies than the centers of the corresponding Co states. As a result of the Co d–Pt d hybridization, the electronic states at the bottom of the valence band are formed mainly by Pt states while the states in the vicinity of the Fermi level (E_F) have predominantly Co

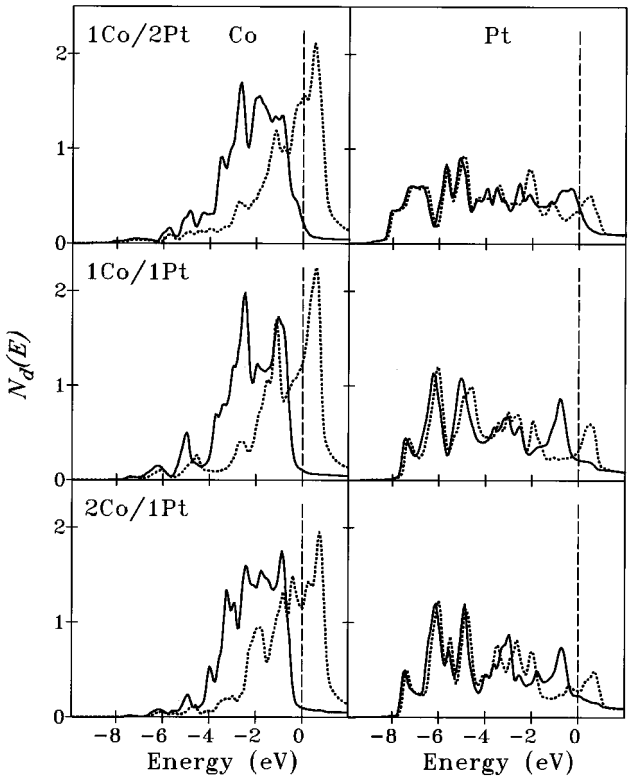

FIG. 4. Spin- and site-projected densities of d states [in units of states/(atom×spin×eV)] for Co and Pt in 1Co/1Pt, 2Co/1Pt, and 1Co/2Pt multilayers. Full and dotted lines correspond to majority and minority spin states, respectively, dashed line marks the Fermi energy.

d character with an admixture of Pt d states. The hybridization with the exchange-splitted Co d states leads to a strong polarization of Pt d states near E_F. The resulting difference in occupation numbers for Pt states with the opposite spin projections gives rise to the appearance of a comparatively large spin magnetic moment at the Pt site.

In the case of the 4Co/2Pt, 2Co/4Pt, and 1Co/5Pt MLS the DOS curves for Co and Pt sites at the interface are similar to the curves shown in Fig. 4. The DOS projected to a site in the interior of the sublayer is close to that of the corresponding bulk metal.

Calculated spin- and site-projected DOS curves for ordered Co_3Pt, CoPt, and $CoPt_3$ alloys are shown in Fig. 5. As compared to the Co/Pt MLS, the electronic structure of the alloys depends much more strongly on the alloy composition. Variation in relative positions of Co and Pt d bands affects the Co d–Pt d hybridization. The valence band width is larger in the Pt-rich alloys due to an increase of the number of Pt nearest neighbors surrounding the Pt site.

Calculated spin m_s and orbital m_l magnetic moments of the Co/Pt multilayers and alloys are summarized in Table II. Both spin and orbital moments at the Co site in the MLS are bigger than in bulk hcp Co with the experimental lattice constant. Nevertheless, from the comparison with the values of m_s and m_l calculated for either hcp or fcc Co with the lattice constant used for the MLS it follows that the moments' enhancement is mainly due to the lattice expansion.

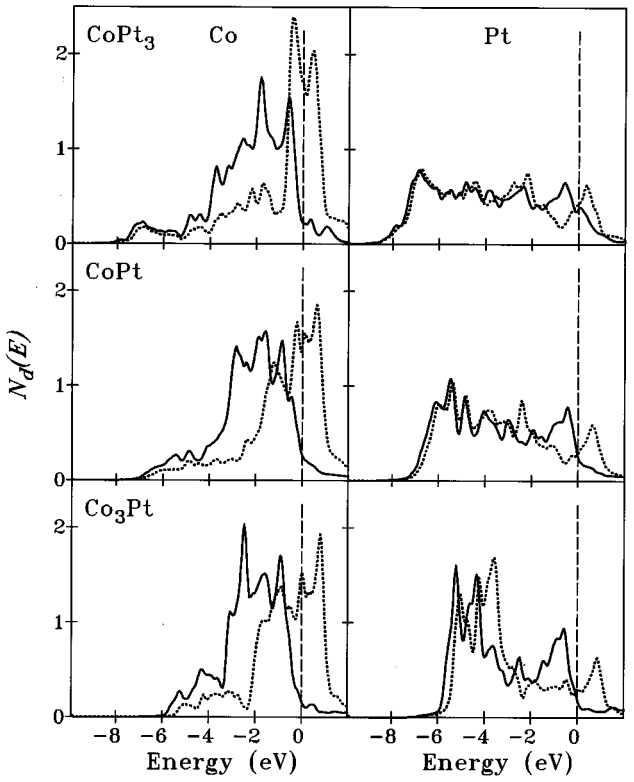

FIG. 5. Spin- and site-projected densities of d states [states/(atom×spin×eV)] for Co and Pt in Co_3Pt, CoPt, and $CoPt_3$ alloys. Full and dotted lines correspond to majority and minority spin states, respectively.

In contrast to the case of the MLS, Co and Pt magnetic moments in the Co-Pt alloys decrease with an increase of Pt contents.

B. Calculated optical and MO properties

When studying the MO properties of the complex Co-Pt compounds it is natural to consider as a reference point the properties of pure Co.[16,39,40] The calculated energy dependence of the polar Kerr rotation angle of fcc Co with the lattice constant $a=3.539$ Å corresponding to the experimental value for hcp Co is shown in Fig. 6 (dashed line). A comparison with the experimental data[4,41] shows that our calculations reproduce correctly the overall shape of the spectra but the uv peak is shifted by about 1 eV to higher energies. The discrepancy is similar to that observed in the theoretical Kerr rotation spectra of Ni[15,42] and is apparently due to a failure of LSDA to describe correctly the width and the spin splitting of d bands in ferromagnetic $3d$ metals. A better agreement with the experiments is obtained for the Kerr rotation calculated with a larger lattice constant $a=3.734$ Å which is equal to the value chosen for all model MLS studied (see solid line in Fig. 6). The increase of the lattice constant results in a narrowing of the d band and, consequently, in an energy scaling of the calculated spectrum. The same tendency has been observed not only for pure Co but also for the Co-Pt alloys and multilayers.

Although the lattice expansion removes the shift of the peaks the calculated amplitude of the peak at 2 eV remains smaller than the experimental one. To elucidate the reason for the discrepancy in amplitudes we examined the dependence of the MOKE spectra on the intraband part of the conductivity tensor. It has been found that in the case of pure Co the Kerr rotation is rather sensitive to the values of γ and ω_p^2 for energies up to 5 eV. Variation of the values changes the amplitude and the position of the uv peak as well as of the peak at 2 eV. The sensitive effect of the Drude term on the uv peak is due to interband contribution to the σ_{xx} being small in this energy range. Thus, though the absolute values of the intraband conductivity are small, its relative contribution is significant. The calculated plasma frequency of hcp

TABLE II. Calculated spin m_s and orbital m_l magnetic moments of the Co/Pt multilayers and alloys. Values in parentheses correspond to the atoms in the layer below the interface. Magnetic moments of hcp Co with the experimental lattice constant $a=2.507$ Å are also given.

	m_s (μ_B/atom)		m_l (μ_B/atom)	
System	Co	Pt	Co	Pt
hcp Co ($a=2.507$ Å)	1.559		0.079	
hcp Co	1.716		0.130	
fcc Co	1.731		0.115	
2Co/1Pt	1.776	0.183	0.098	0.019
1Co/1Pt	1.752	0.255	0.089	0.028
1Co/2Pt	1.880	0.207	0.099	0.022
4Co/2Pt	1.810	0.192	0.103	0.018
	(1.738)		(0.104)	
2Co/4Pt	1.765	0.154	0.095	0.016
		(0.049)		(0.001)
1Co/5Pt	1.869	0.175	0.090	0.018
		(0.058)		(0.006)
Co_3Pt	1.735	0.339	0.087	0.083
CoPt	1.681	0.321	0.090	0.048
$CoPt_3$	1.607	0.199	0.027	0.035

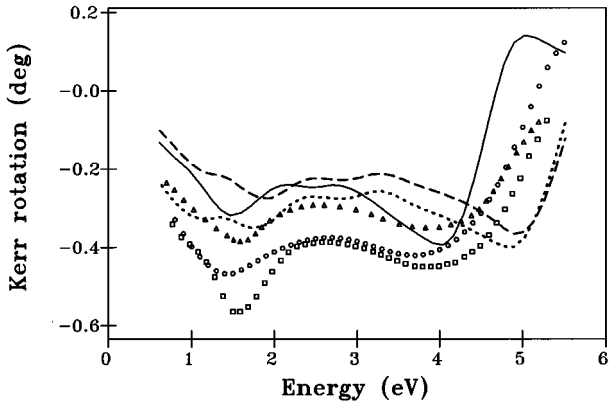

FIG. 6. Experimental and theoretical polar Kerr rotation spectra of Co. The theoretical Kerr rotation spectra of fcc Co calculated using the experimental lattice constant and with the plasma frequency in the Drude term taken from the calculations (dashed curve), with $\hbar\omega_p=5$ eV (dotted curve), and calculated using the same lattice constant as for the Co/Pt MLS (solid curve). Experimental spectra are shown by circles (present work), squares (Ref. 41), and triangles (Ref. 4).

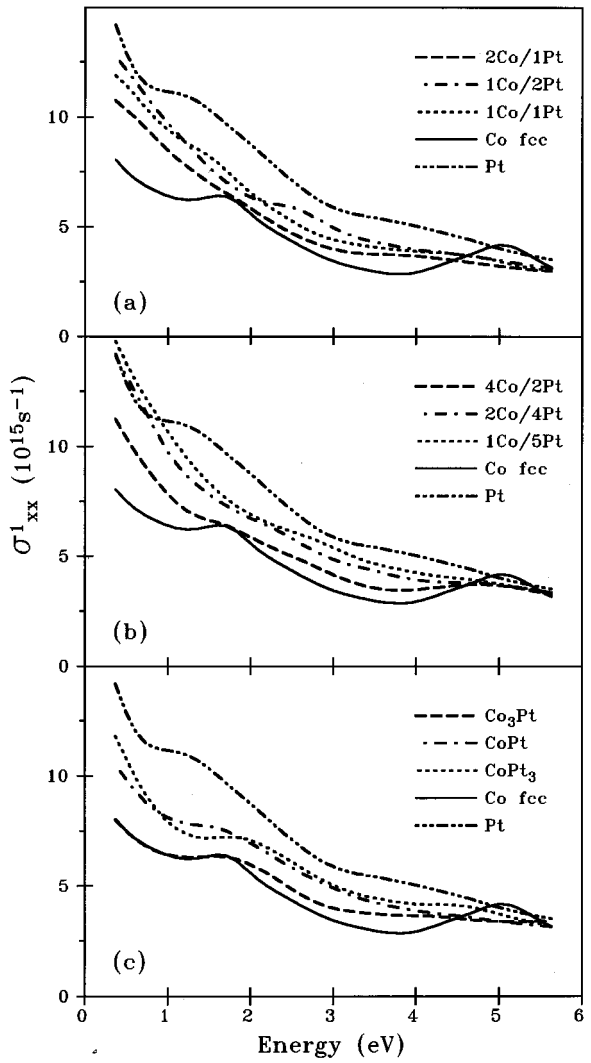

FIG. 7. Theoretical $\sigma_{xx}^{(1)}$ spectra of the Co/Pt multilayers [(a) and (b)], and alloys (c).

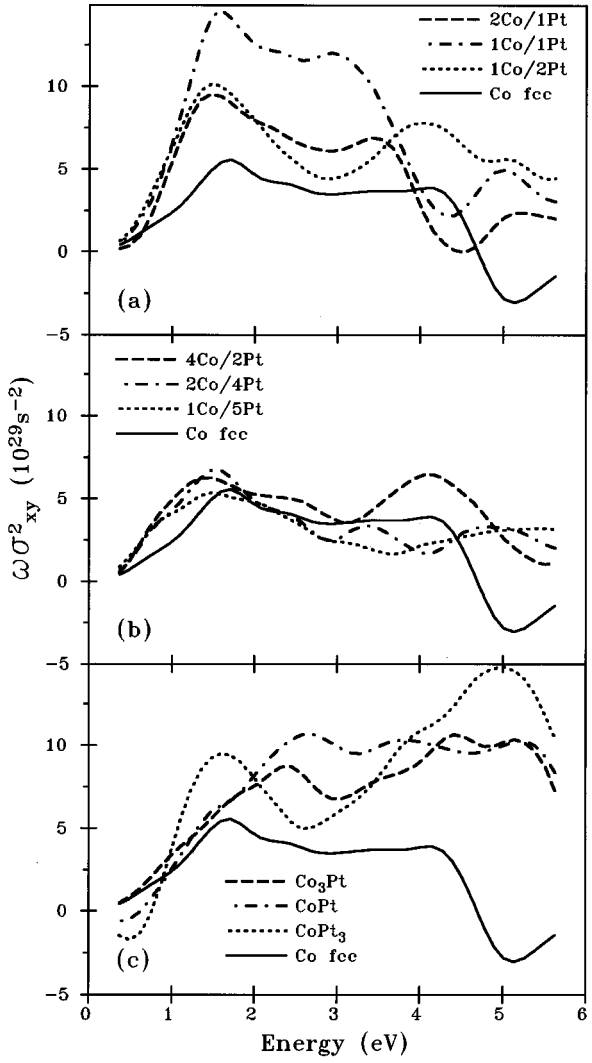

FIG. 8. Theoretical $\omega\sigma_{xy}^{(2)}$ spectra of the Co/Pt multilayers [(a) and (b)], and alloys (c).

Co with the experimental lattice constant was found to be 7.2 eV and the experimental value for the hcp Co single crystal is ~ 5 eV.[43] Such discrepancy is in agreement with the previous observation[44] that the calculated values of ω_p are, as a rule, 20–50 % higher than the experimental values. The polar Kerr rotation calculated with $\hbar\omega_p = 5$ eV is shown by the dotted line in Fig. 6. The use of the smaller value of ω_p leads to a better agreement with the experiment. Nevertheless, we could not manage to achieve close agreement with the experiment in the ir range varying the Drude constants in reasonably wide limits. It has been found that for the Co/Pt multilayers and alloys the dependence of MOKE on the intraband contribution is much weaker, and in the following we use calculated values of ω_p to evaluate the intraband conductivity.

Theoretical results for the absorptive part of the conductivity tensor $\sigma_{xx}^{(1)}$ for fcc Co, Pt, and some model Co/Pt multilayers and alloys are shown in Fig. 7. For energies higher than 1.5 eV $\sigma_{xx}^{(1)}$ of the MLS and the alloys have similar energy dependence and fall within the range between $\sigma_{xx}^{(1)}$ curves of bulk Co and Pt, the conductivity of Co-rich MLS being closer to $\sigma_{xx}^{(1)}$ of Co.

The calculated dependence of $\sigma_{xx}^{(1)}$ on Co contents correlates well with the data obtained from the ellipsometric measurements of Co/Pt multilayers with different Co-layer thickness. Although the calculations give $\sigma_{xx}^{(1)}$ of a higher amplitude than the experimental data, the theoretical results reproduce the changes of $\sigma_{xx}^{(1)}$ with the variation of the Co sublayer thickness. Of all the MLS considered, only $\sigma_{xx}^{(1)}$ of 4Co/2Pt has a subtle feature at ~ 5 eV corresponding to bulk Co. The fact that the σ_{xx} curves of the Co-Pt compounds of different composition and of different chemical ordering have similar shapes with no pronounced features suggests that, unlike the case of bulk Co, the two-peaks structure of the polar Kerr rotation spectra of Co/Pt MLS comes from the energy dependence of the off-diagonal part of the conductivity tensor.

The results of the calculations of the absorptive part of $\omega\sigma_{xy}$ of Co/Pt MLS and alloys are shown in Fig. 8. The calculated $\omega\sigma_{xy}^{(2)}$ of pure fcc Co is shown by the solid curve in all figures for reference sake. All the compounds can be divided into three distinct groups according to differences between their $\omega\sigma_{xy}^{(2)}$ and that of pure Co. The first group

consists of 2Co/1Pt, 1Co/1Pt, and 1Co/2Pt multilayers [Fig. 8(a)], which have no more than two consecutive planes of equivalent atoms. For these MLS the energy dependence of $\omega\sigma_{xy}^{(2)}$ varies strongly with MLS composition, with the absolute values of $\omega\sigma_{xy}^{(2)}$ being significantly larger compared to Co. In the case of 2Co/1Pt and 1Co/1Pt the curves have the similar shape, but $\omega\sigma_{xy}^{(2)}$ of the latter is $\sim$1.5 times greater. The position of the peak at $\sim$1.5 eV is not altered compared to Co, while the feature at $\sim$3.5 eV is shifted to lower energies by 1 eV and an additional peak appears around 5.5 eV. There are two maxima in $\omega\sigma_{xy}^{(2)}$ of 1Co/2Pt, which lies at approximately the same energies as in Co, but their intensities are two times higher.

The situation is quite different in the case of multilayers with greater sublayer thickness [Fig. 8(b)]. Some increase in $\omega\sigma_{xy}^{(2)}$ is observed only for 4Co/2Pt MLS, with the shape of the curve being similar to that of Co. The $\omega\sigma_{xy}^{(2)}$ of 2Co/4Pt and 1Co/5Pt lies very close to each other and are reduced compared to $\omega\sigma_{xy}^{(2)}$ of Co in the energy range of 2.5–4.5 eV. It should be noted that the two last MLS have Co and Pt sublayer thicknesses which are close to those of experimentally studied films.

Our results for 2Co/1Pt and 2Co/4Pt multilayers are somewhat different from those given in Ref. 18. The discrepancy is partially due to slightly different values of structural parameters. Nevertheless, calculations performed with the same parameters as in Ref. 18 show that the difference between the two calculations disappears only when the combined corrections to the LMTO Hamiltonian and overlap matrices are not included. This is not surprising, because even with the current density matrix elements computed accurately, the neglect of the combined corrections terms affect the calculated conductivity tensor via changes in band energies.

The calculated $\omega\sigma_{xy}^{(2)}$ for model alloys are shown in Fig. 8(c). The common feature of all the spectra is a strong enhancement of $\omega\sigma_{xy}^{(2)}$ in the energy range 4–6 eV. Of the three curves, $\omega\sigma_{xy}^{(2)}$ for $CoPt_3$ is of a different shape with two distinct maxima at $\sim$1.5 and 5 eV, the amplitude of the latter being more than three times greater than the feature in the spectrum of Co at $\sim$4.5 eV.

It has been shown[31,42] that in pure $3d$ metals the off-diagonal conductivity is proportional to the strength of the spin-orbit coupling. In transition-metal compounds, however, the dependence of the MO properties on the spin-orbit coupling and effective magnetization of constituent atoms is far more complicated.[45] To understand this better we performed model calculations with the spin-orbit coupling set to zero on either Co or Pt site. It has been found that ''switching off'' the spin-orbit coupling inside the Co atomic sphere affects only slightly the off-diagonal part of the conductivity tensor, while neglecting the spin-orbit interaction in the Pt sphere results in a strong decrease of $\omega\sigma_{xy}^{(2)}$. These results are in qualitative agreement with those obtained by the authors of Ref. 46, who also observed a strong dependence of $\omega\sigma_{xy}^{(2)}$ on the value of the spin-orbit coupling on the Pt site. Besides, we investigated the effect of excluding the matrix elements of the effective magnetic field on Co and Pt sites from the LMTO Hamiltonian. When the matrix elements on the Co sphere are zero the off-diagonal part of the conductivity decreases drastically. At the same time, ''switching off'' the effective magnetic field on the Pt site produces a negligible effect on the $\omega\sigma_{xy}^{(2)}$ spectra. Thus, a strong spin-orbit coupling on only one of the inequivalent atomic sites and a large value of the effective magnetization on another one can be sufficient for alloys to manifest strong MO activity.

In addition, it has been found that the dominant contribution to the $\omega\sigma_{xy}^{(2)}$ spectra in the energy range of interest (1–6 eV) comes from transitions to unoccupied states lying in a rather narrow energy interval of $\sim$1 eV just above the E_F. At the same time, these transitions give relatively small contribution to the diagonal part of the optical conductivity. As has been mentioned above, the electronic states in the vicinity of the E_F are formed by strongly hybridized Co d and Pt d states.

It is worthwhile to note, that in the case of transition-metal compounds, wave functions of initial and final states involved in optical transition are delocalized. Consequently, it is difficult, if possible at all, to separate contributions of any intra- or interatomic transitions to MO spectra. The assumption that the enhanced MO effects in Co/Pt compounds are due to Co d–Pt d hybridization allows us to explain the relatively small (as compared to Co/Pt alloys) magnitude of calculated $\omega\sigma_{xy}^{(2)}$ in 2Co/4Pt and 1Co/5Pt multilayers. In these MLS there are Pt layers consisting of atoms which have Co atoms among neither the first nor the second nearest neighbors and the contribution of these layers to $\omega\sigma_{xy}^{(2)}$ is small. However, switching off the spin-orbit interaction for these atoms leads to a rather strong variation of the spectrum. Neglecting the spin-orbit coupling for Pt atoms at Co-Pt interface only leads to relatively pronounced changes, but the magnitude of $\omega\sigma_{xy}^{(2)}$ remains considerably higher than the magnitude of $\omega\sigma_{xy}^{(2)}$ calculated with the spin-orbit interaction at all Pt atoms set to zero.

Calculated polar Kerr rotation spectra are shown in Fig. 9. From a comparison with the experimental MOKE spectra of Co/Pt MLS shown in Fig. 1 it can be seen that the calculated spectra of MLS do not satisfactorily reproduce the experimental data. The magnitude of the calculated MOKE spectra of 2Co/4Pt and 1Co/5Pt MLS [Fig. 9(b)] in the energy range of 3–5 eV is significantly smaller than that of pure Co while an enhancement of the rotation angle of MLS vs pure Co is observed in the experiment. The enhancement is indeed found for Co/Pt MLS with smaller sublayer thickness [Fig. 9(a)] but in contrast to the experimental data the peak is shifted to lower energy with respect to its position in Co. Surprisingly, better agreement with the experimentally observed MOKE spectra is observed in the case of Co-Pt alloys [Fig. 9(c)]. The calculated spectra reproduce fairly well both the increase of magnitude and the shift of the uv peak to higher energies.

The discrepancy between the experimental Kerr rotation spectra of Co/Pt MLS obtained in the present work and the calculated spectra of the model Co/Pt multilayers may be due to inadequacy of the adopted structure model of the MLS with the sharp interlayer interface. The observed energy dependence of the MOKE spectra of the MLS and their variation with the Co sublayer thickness may be explained by the reasonable assumption that a Co-Pt alloy is formed at the interface.

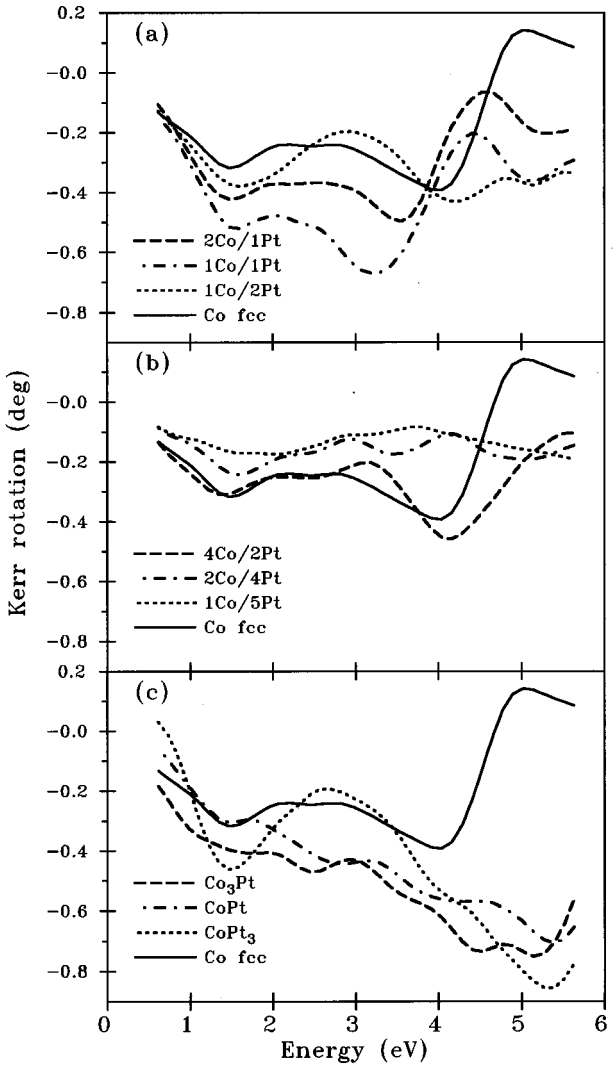

FIG. 9. Theoretical polar Kerr rotation spectra of the Co/Pt multilayers [(a) and (b)], and alloys (c).

It is interesting to compare the results of our calculations with the recently published polar Kerr rotation spectra of an artificial Co_3Pt alloy film.[47] X-ray-diffraction data show that after annealing at 650 K the alloy consists of an alternating sequence of closely packed Co and Co-Pt planes with hcp-like kind of stacking. Due to existence of the well-defined order along the crystallographic *c* direction the structure of the alloy is rather close to that of the model 1Co/1Pt multilayer. Nevertheless, because of different compositions of the two compounds, the direct comparison of the experimental and calculated MOKE spectra should be made with care. Calculated MOKE spectra of 1Co/1Pt multilayers with *ababab* and *abcabc* layer sequences are shown in Fig. 10 together with the experimental spectra. Except in the ir range, the calculated spectra are similar, with slightly different amplitudes. Both theoretical spectra have a peak at ~ 3 eV which is clearly seen in the experimental curve. A 5 eV feature in the experimental spectrum is also reproduced by the calculations but corresponding peaks are slightly shifted to higher energies. The shift may be caused by the difference of experimental and theoretical lattice constants. After annealing at 950 K the Co_3Pt alloy film has been shown to consist of a chemically disordered fcc phase. The modification of atomic arrangement and chemical short-range order causes significant changes of the observed MOKE spectra. The 3 eV peak disappears while the amplitude of the spectra in the uv range increases and the 5 eV feature transforms into a peak. Similar changes are readily seen when comparing the calculated MOKE spectra of 1Co/1Pt multilayers with the calculated spectrum of Co_3Pt alloy.

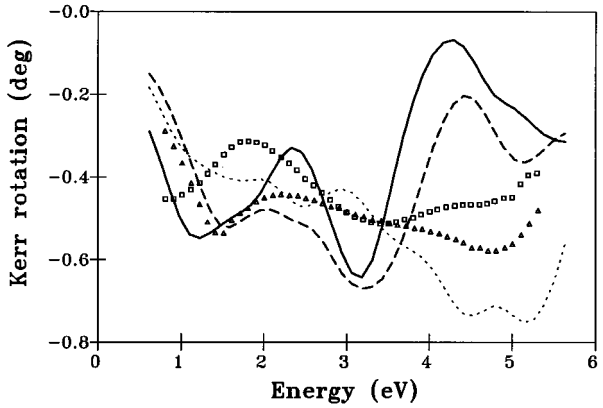

FIG. 10. Theoretical polar Kerr rotation spectra of 1Co/1Pt multilayers with *ababab* (solid line) and *abcabc* (dashed line) stacking. Calculated spectrum of Co_3Pt alloy is shown by the dotted line. Experimental spectra for ordered hexagonal Co_3Pt phase (squares) and chemically disordered fcc phase (triangles) are taken from Ref. 47.

In conclusion it should be pointed out that the Kerr rotation of Co/Pt MLS is governed mainly by the off-diagonal part of the conductivity tensor. The infrared part of the spectrum originates from the MO activity of Co layers itself and is scaled by its contents. On the other hand, the peak in the uv region is due to the hybridization of strongly spin-polarized Co *d* states with spin-orbit-splitted Pt *d* states and its magnitude weakly depends on the MLS composition. It has been demonstrated that the chemical and structural ordering is accompanied by substantial electronic structure changes and results in a drastic MOKE spectra modification.

It should be noted that the *ab initio* description of the MOKE spectra for model Co/Pt multilayers performed under the assumption of a sharp, ideal interface is not sufficiently adequate for the detailed explanation of the experimentally observed ones. Simultaneously, in the case of model Co-Pt alloys the calculations properly reflect the main features of the spectra observed experimentally. Thus it can be concluded that in the real multilayer structures the limited interdiffusion region at the interface and its structure and chemical composition play a main role in the formation of the MO spectra of the Co/Pt MLS.

ACKNOWLEDGMENTS

The authors are grateful to Dr. P. M. Oppeneer for many helpful discussions. The research described in this publication was made possible in part by Grant No. U42000 from the International Science Foundation.

*Permanent address: Institute of Metal Physics, 36 Vernadskii str., 252142 Kiev, Ukraine.

[1] S. S. P. Parkin, N. More, and K. P. Roche, Phys. Rev. Lett. **64**, 2304 (1990).

[2] M. N. Baibich, J. M. Broto, A. Fert, F. Nguyen Van Dau, F. Petroff, P. Etienne, G. Creuzet, A. Friederich, and J. Chazelas, Phys. Rev. Lett. **61**, 2472 (1988).

[3] M. G. Samant, J. Stöhr, S. S. S. Parkin, G. A. Held, B. D. Hermsmeier, F. Herman, M. van Schilfgaarde, L.-C.Duda, D. C. Mancini, N. Wassdahl, and R. Nakajima, Phys. Rev. Lett. **72**, 1112 (1994).

[4] W. B. Zeper, F. J. A. M. Greidanus, P. F. Carcia, and C. R. Fincher, J. Appl. Phys. **65**, 4971 (1989).

[5] D. Weller, W. Reim, K. Spörl, and H. Brändle, J. Magn. Magn. Mater. **93**, 183 (1991).

[6] C.-J. Lin, G. L. Gorman, C. H. Lee, R. F. C. Farrow, E. E. Marinero, H. V. Do, H. Notarys, and C. J. Chien, J. Magn. Magn. Mater. **93**, 194 (1991).

[7] K. Sato, H. Ikekame, Y. Tosaka, K. Tsuzukiyama, Y. Togami, and M. Fujisawa, J. Magn. Magn. Mater. **126**, 572 (1993).

[8] H. Brändle, D. Weller, J. C. Scott, S. S. P. Parkin, and C.-J. Lin, IEEE Trans. Magn. **MAG-28**, 2967 (1992).

[9] K. Sato, H. Hongu, H. Ikekame, J. Watanabe, K. Tsuzukiyama, Y. Togami, M. Fujisawa, and T. Fukazawa, Jpn. J. Appl. Phys. **31**, 3603 (1992).

[10] S. Visnovsky, M. Nyvlt, V. Parizek, P. Kielar, V. Prosser, and R. Krishnan, IEEE Trans. Magn. **MAG-29**, 3390 (1993).

[11] J. Zak, E. R. Moog, C. Liu, and S. D. Bader, Phys. Rev. B **43**, 6423 (1991).

[12] S. Uba, L. Uba, and R. Gontarz, IEEE Trans. Magn. **MAG-30**, 806 (1994).

[13] S. Uba, L. Uba, R. Gontarz, and Yu. V. Kudryavtsev (unpublished).

[14] P. N. Argyres, Phys. Rev. **97**, 334 (1955).

[15] P. M. Oppeneer, T. Maurer, J. Sticht, and J. Kübler, Phys. Rev. B **45**, 10 924 (1992).

[16] V. N. Antonov, A. Ya. Perlov, A. P. Shpak, and A. N. Yaresko, J. Magn. Magn. Mater. **146**, 205 (1995).

[17] S. Uba, L. Uba, R. Gontarz, V. N. Antonov, A. Ya. Perlov, and A. N. Yaresko, J. Magn. Magn. Mater. **140-144**, 575 (1995).

[18] G. Y. Guo and H. Ebert, Phys. Rev. B **51**, 12 633 (1995).

[19] T. Kusakabe, K. Kyuno, and S. Asano, J. Magn. Magn. Mater. **126**, 535 (1993).

[20] L. Smardz, J. Baszynski, and B. Rauschenbach, Thin Solid Films **175**, 295 (1989).

[21] K. Sato, Jpn. J. Appl. Phys. **20**, 2403 (1981).

[22] D. E. Aspnes and A. A. Studna, Appl. Opt. **14**, 220 (1975).

[23] O. K. Andersen, Phys. Rev. B **12**, 3060 (1975).

[24] V. V. Nemoshkalenko, A. E. Krasovskii, V. N. Antonov, Vl. N. Antonov, U. Fleck, H. Wonn, and P. Ziesche, Phys. Status Solidi B **120**, 283 (1983).

[25] H. Ebert, Phys. Rev. B **38**, 9390 (1988).

[26] V. N. Antonov, A. I. Bagljuk, A. Ya. Perlov, V. V. Nemoshkalenko, Vl. N. Antonov, O. K. Andersen, and O. Jepsen, Low Temp. Phys. **19**, 494 (1993).

[27] K. H. J. Buschow, in *Ferromagnetic Materials*, edited by K. H. J. Buschow and E. P. Wohlfarth (North-Holland, Amsterdam, 1988), Vol. 4, p. 493.

[28] W. Reim and J. Schoenes, in *Ferromagnetic Materials*, edited by K. H. J. Buschow and E. P. Wohlfarth (North-Holland, Amsterdam, 1990), Vol. 5, p. 133.

[29] R. Kubo, J. Phys. Soc. Jpn. **12**, 570 (1957).

[30] C. S. Wang and J. Callaway, Phys. Rev. B **9**, 4897 (1974).

[31] Yu. A. Uspenskii and S. V. Khalilov, Zh. Éksp. Teor. Fiz. **95**, 1022 (1989) [Sov. Phys. JETP **68**, 588 (1989)].

[32] G. Lehmann and M. Taut, Phys. Status Solidi B **54**, 469 (1972).

[33] S. Doniach, in *Optical Properties and Electronic Structure of Metals and Alloys*, edited by F. Abeles (North-Holland, Amsterdam, 1966).

[34] The MOKE spectrum of the Co film presently studied differs from that previously published in Ref. 17 due to the smaller film thickness of the latter and known dependencies of MOKE on the film microstructure, see, e.g., T. Suzuki, D. Weller, C.-A. Chang, R. Savoy, T. Huang, B. A. Gurney, and V. Speriosu, Appl. Phys. Lett. **64**, 2736 (1994).

[35] D. E. Aspnes, in *Handbook of Optical Constants of Solids*, edited by E. D. Palik (Academic, Orlando, FL, 1985).

[36] S. Logothetidis, S. Boultadakis, N. K. Flevaris, and D. Fuchs, J. Magn. Magn. Mater. **93**, 444 (1991).

[37] U. von Barth and L. A. Hedin, J. Phys. C **5**, 1629 (1972).

[38] P. E. Blöchl, O. Jepsen, and O. K. Andersen, Phys. Rev. B **49**, 16 223 (1994).

[39] P. M. Oppeneer, T. Kraft, and H. Eschrig, Phys. Rev. B **52**, 3577 (1995).

[40] G. Y. Guo and H. Ebert, Phys. Rev. B **50**, 10 377 (1994).

[41] D. Weller, G. R. Harp, R. F. C. Farrow, A. Cebollada, and J. Sticht, Phys. Rev. Lett. **72**, 2097 (1994).

[42] P. M. Oppeneer, J. Sticht, T. Maurer, and J. Kübler, Z. Phys. B **88**, 309 (1992).

[43] M. M. Kirillova, G. A. Bolotin, and L. V. Nomerovannaya, Opt. Spectrosc. **49**, 742 (1980).

[44] S. N. Rashkeev, Yu. A. Uspenskii, and I. I. Mazin, Zh. Éksp. Teor. Fiz. **88**, 1687 (1985) [Sov. Phys. JETP **61**, 1004 (1985)].

[45] P. M. Oppeneer, V. N. Antonov, T. Kraft, H. Eschrig, A. N. Yaresko, and A. Ya. Perlov, Solid State Commun. **94**, 255 (1995).

[46] D. Weller, J. Sticht, G. R. Harp, R. F. C. Farrow, R. F. Marks, and H. Brändle, in *Magnetic Ultrathin Films—Multilayers and Surfaces, Interfaces and Characterization*, edited by B. T. Jonker, S. A. Chambers, R. F. C. Farrow, C. Chappert, R. Clarke, W. J. M. de Jonge, T. Egami, P. Grünberg, K. M. Krishnan, E. E. Marinero, C. Rau, and S. Tsunashima, MRS Symposia Proceedings No. 313 (Materials Research Society, Pittsburgh, 1993), p. 501.

[47] G. R. Harp, D. Weller, T. A. Rabedeau, R. F. C. Farrow, and M. F. Toney, Phys. Rev. Lett. **71**, 2493 (1993).